Sinuous gullies on Mars: Frequency, distribution, and implications for flow properties

N. Mangold,[1] A. Mangeney,[2] V. Migeon,[1] V. Ansan,[1] A. Lucas,[2] D. Baratoux,[3] and F. Bouchut[4]

Received 13 November 2009; revised 4 March 2010; accepted 2 June 2010; published 5 November 2010.

[1] Recent gullies on Mars are suspected to be the result of liquid-water-bearing flows. A formation from wet flows has been challenged by studies invoking granular (dry) flows. Our study focuses on the sinuous shapes observed for some of the recent Martian gullies. Sinuous gullies are found in locations and slopes (of 10°–15°) similar to straight gullies, and they are therefore related to the same formation processes. Numerical simulations of granular flows are performed here by introducing topographic variations such as obstacles, roughness, or slope changes that could possibly generate flow sinuosity. None of these simulations was able to reproduce sinuous shapes on a slope lower than 18° with friction angles typical of dry granular material. The only way to simulate sinuous shapes is to create small-amplitude periodic variations of the topography of the deposit, an origin not supported by current Martian imagery. Given the presence of sinuosity in natural terrestrial debris flows, we have concluded that sinuous Martian gullies are better reproduced by liquid-water-bearing debris flows. Sinuous shapes in leveed flows are used to derive mechanical parameters from several Martian gullies using photoclinometry. Values in yield strength of 100–2200 Pa, velocities of 1.1–3.3 m s^{-1}, and viscosities from 40 to 1040 Pa s are found, which are all within the range of values for terrestrial debris flows with various proportions of liquid water (20%–40%).

Citation: Mangold, N., A. Mangeney, V. Migeon, V. Ansan, A. Lucas, D. Baratoux, and F. Bouchut (2010), Sinuous gullies on Mars: Frequency, distribution, and implications for flow properties, *J. Geophys. Res.*, *115*, E11001, doi:10.1029/2009JE003540.

1. Introduction

[2] Liquid water is unlikely to persist on the surface of Mars under current atmospheric conditions [*Ingersoll*, 1970; *Haberle et al.*, 2001]. However, geologically recent Martian hillside gullies, discovered using Mars Orbiter Camera (MOC) Narrow Angle (NA) images [*Malin and Edgett*, 2000], exhibit characteristic morphologies similar to terrestrial features formed by flowing water or water-rich slurries, a finding that led *Malin and Edgett* [2000] to suggest that they formed by the action of water. Observations based on gully morphology have confirmed that liquid water mixed in debris flows can explain the shape of gullies [e.g., *Costard et al.*, 2002; *Mangold et al.*, 2003]. However, the cause of melting remains controversial. A subsurface origin was proposed in the original publication by *Malin and Edgett* [2000]. An atmospheric control was proposed in other models [e.g., *Costard et al.*, 2002; *Christensen*, 2003; *Levy et al.*, 2009]. Processes other than liquid water erosion have also been proposed to explain the formation of gullies, including the action of CO_2-based debris flows [*Hoffman et al.*, 2000; *Musselwhite et al.*, 2001], dry granular avalanches [*Treiman*, 2003; *Shinbrot et al.*, 2004], or the mass wasting of CO_2 frost [*Ishii and Sasaki*, 2004]. Reasons that several researchers have interpreted these flows as granular flows include the overall morphology of gullies, showing an alcove, a channel, and a debris fan that can be replicated by simple dry granular flows in a laboratory [*Shinbrot et al.*, 2004]. In fact, many characteristics of (dry) granular flows, such as channels and levees, are similar to those of the mass wasting of viscous slurries containing liquid water [*Felix and Thomas*, 2004; *Mangeney et al.*, 2007a], which creates ambiguity regarding the understanding of gullies and raises questions regarding their origins by dry or wet processes [e.g., *Treiman*, 2003].

[3] Our goal is to study gullies on Mars that display locally sinuous channels. Our study aims to (1) determine if sinuous channels and the more common straight gullies are produced by similar processes, by determining their distribution, orientation, and slope; (2) use granular flow modeling to identify the ability of granular flows to display sinuosity on observed

[1]Laboratoire de Planétologie et Géodynamique de Nantes, Université de Nantes, CNRS, Nantes, France.
[2]Institut de Physique du Globe de Paris, Université Paris Diderot 7, CNRS, Paris, France.
[3]Observatoire Midi-Pyrénées, Université Toulouse III, CNRS, Toulouse, France.
[4]École Normale Supériere, CNRS, Paris, France.

Copyright 2010 by the American Geophysical Union.
0148-0227/10/2009JE003540

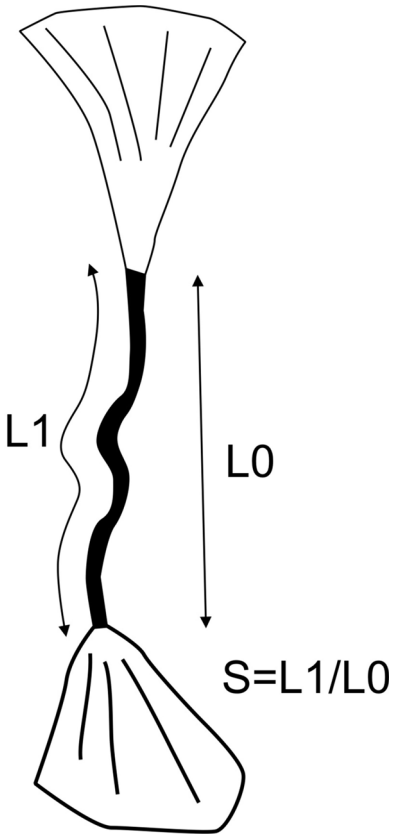

Figure 1. Sketch of one typical gully with its (top) alcove, (middle) channel, and (bottom) debris fan. The sinuosity index (*S*) is measured as the ratio between the channel length (L1) and the straight line joining the channel top and bottom (L0).

slopes; and (3) estimate the physical properties of the flows (velocity, viscosity) from specific sinuous leveed channels.

2. Morphology and Distribution of Sinuous Gullies on Mars

2.1. Sinuous Gully Morphometry and Frequency

[4] Martian gullies are incised into hillslopes in terrains such as impact crater walls, valleys, pits, knobs, buttes, hills, and escarpments [e.g., *Balme et al.*, 2006]. They comprise three identifiable components: alcoves, channels, and depositional fans (Figure 1). The uppermost components of gullies and alcoves are generally located below or at the brink of the host slope. They presumably represent the source region for the flow and are likely formed by backward erosion. Alcoves frequently narrow downslope [*Treiman*, 2003; *Heldmann and Mellon*, 2004] and sometimes contain boulders, up to tens of meters in diameter, or other in-filling material. Channels, generally up to a few tens of meters in width [*Mellon and Phillips*, 2001] and up to a few kilometers in length [*Heldmann and Mellon*, 2004], begin at the base of the alcoves, are incised into hillslopes, and often dissect lower depositional aprons where they terminate. They often become narrower and shallower downslope. The transition between a channel and an apron is either found via a distributary network incised into the apron, an abrupt termination at a depositional flow, or a gradual fading of the channel into apron deposits.

[5] Among channels observed in gullies, some are sinuous. The sinuosity index *S* is the ratio between the total channel length (L1) and the straight line from the top to the bottom of each channel (L0) (Figure 1). Gullies display diverse shapes, from those exhibiting one or two bends to some displaying a series of bends similar to meanders of a river (Figures 2 and 3). We measured the sinuosity of gullies in 250 MOC images from both hemispheres. By taking the whole channel length, we underestimate local high sinuosities of channels that may be locally more sinuous in one subsection of the channel than in others, but the average value for the whole channel is accurate enough to distinguish sinuous channels from straight channels.

[6] MOC imagery, typically at 2.8 m/pixel, may be locally too coarse to get a precise measurement of channel sinuosity. To achieve accurate statistics, MOC images were compared to two High Resolution Imaging Science Experiment (HiRISE) [*McEwen et al.*, 2007] images for the same location (Figures 2 and 3). In Figure 2, the sinuosity indexes of channels A, B, and C are measured at 1.11, 1.07, and 1.06, respectively, in the MOC image and at 1.12, 1.10, and 1.08 in the HiRISE image. In Figure 3, the sinuosity indexes of channels A and B are, respectively, 1.23 and 1.19 in the MOC image and 1.26 and 1.24 in the HiRISE image. The examples indicate that the measurement in MOC images underestimates the sinuosity index compared with HiRISE images by only a few percent. In addition, straight gullies appear straight in both images, indicating that different camera phase angles are not responsible for a deformation sufficient to display gullies as sinuous. Given these results and since HiRISE images are not yet sufficiently numerous to give a statistical view of Martian gullies, the MOC imagery is used to measure the sinuosity index for most gullies. A large majority of the 250 MOC images has a 2.8 m/pixel resolution, guaranteeing a homogeneous result.

[7] A total of approximately 3600 individual gully channels are present in the 250 MOC images studied (Figure 4). Indexes larger than 1.05 represent a sinuosity that could be identified by visual observations: this value is chosen as the minimum value for a gully to be defined as sinuous. Indexes higher than 1.20 represent a meandering-like channel (as seen in Figure 3). A total of 3.5% of individual gullies display an index larger than 1.05, with approximately 25% of images containing at least one sinuous gully ($S > 1.05$). A decrease in the number of sinuous gullies with an increase in the sinuosity index indicates that highly sinuous channels are not common. We also plotted the sinuosity percentage, which corresponds to the percentage of channel lengths longer than a straight line that is directly extracted from the index (when $S = 1.20$, the percentage is 20%). The plot in the log-log axes shows curves close to straight lines, which means that the sinuosity index is close to a power law distribution.

[8] Since both statistical tools (individual gullies and images containing sinuous gullies) display the same trend, a study for the distribution of sinuous gullies is hereafter presented by the total number of images containing at least one sinuous gully, because it is accurate enough to represent the geographic distribution of gullies. Indeed, the goal of

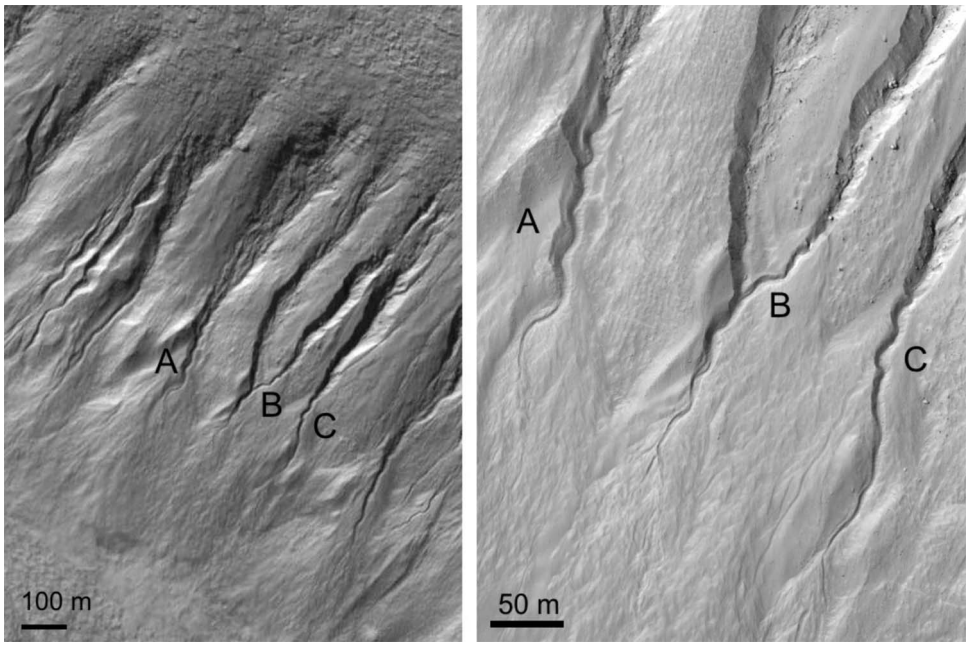

Figure 2. (left) MOC image E18-00685 (phase angle 48.3°). (right) HiRISE image PSP_005930_1395 (phase angle 49.5°). The sinuosity indexes of channels A, B, and C are, respectively, 1.11, 1.07, and 1.06 in the MOC image and 1.12, 1.10, and 1.08 in the HiRISE image.

section 2.2 is to observe if sinuous gullies are typical of the location where straight gullies are found, but not to map the highest density of individual sinuous gullies on Mars.

2.2. Geographic Distribution, Elevation, Orientation, and Slopes of Sinuous Gullies

[9] In general, gullies are more common in the southern hemisphere than in the northern hemisphere, but they occur in both hemispheres more frequently between 30° and 50° in latitude [*Malin and Edgett*, 2000, 2001; *Costard et al.*, 2002; *Miliken et al.*, 2003; *Heldmann and Mellon*, 2004; *Balme et al.*, 2006]. Studies have reported an almost complete absence of gullies near the equator, which is also observed in our mapping (Figure 5a). Sinuous gullies are present in almost all regions containing straight gullies. In the region of the Newton basin and its vicinity (190°E, 30°S–40°S), a region of abundant straight gully occurrences, a high frequency of highly sinuous gullies was also determined.

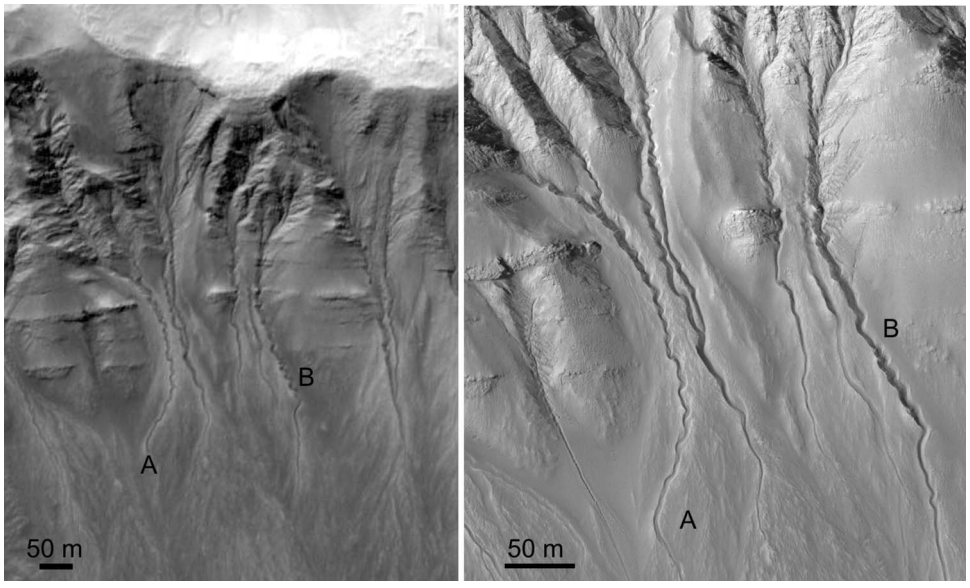

Figure 3. (left) MOC image E16-00043 (phase angle 35°). (right) HiRISE image PSP_003464_1380 (phase angle 54.9°). The sinuosity index of channels A and B are, respectively, 1.23 and 1.19 in the MOC image and 1.26 and 1.24 in the HiRISE image.

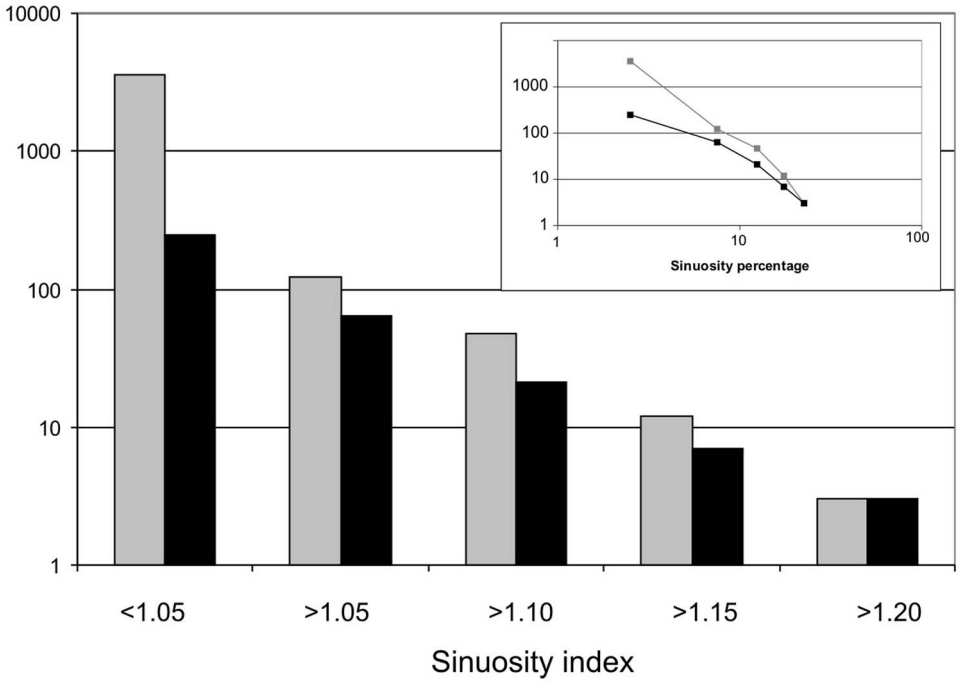

Figure 4. Histogram of gully sinuosity occurrences in 250 MOC images. The number of images with a corresponding sinuosity index, is shown in black, taking the highest sinuosity index occurrence in each image. The number of individual gullies with a corresponding sinuosity index is shown in gray. At the top right the sketch shows a log-log plot for the percentage of sinuosity versus the number of images, taking the highest sinuosity index occurring in each image.

[10] The elevations of gullies were taken automatically using Mars Observer Laser Altimeter (MOLA) data with MOC image coordinates (Figure 5b). The method does not provide high precision on the elevation, but it is enough to compare the distribution of straight and sinuous gullies with elevation. Straight gullies are scattered at various elevations. Sinuous gullies also occur over a large variety of elevations, without a preference for one range in elevation. The highest occurrences of sinuous channels occur at elevations ranging from 500 to 1500 m, where the highest occurrences of straight gullies are also found. Sinuous gullies do not often occur at low elevations. Such elevations correspond to the northern hemisphere, where the geographic distribution also confirms the minority of sinuous channels (Figure 5a), which display sinuosity indexes below 1.10.

[11] The global distribution of gully orientations is complex. Initial studies have suggested that pole-facing gullies were the most common [*Malin and Edgett*, 2000; *Costard et al.*, 2002], but as more data have been acquired, the picture has become more complicated: equator-facing gullies seem to be more common in the high northern latitudes, but not in northern midlatitudes [*Bridges and Lackner*, 2005]; pole-facing gullies are predominant in the southern midlatitudes, but not much farther south [*Berman et al.*, 2005; *Balme et al.*, 2006]. Figures 5c–5e display the result of orientations for the southern hemisphere only (statistics for the north would not be significant). As with straight gullies, sinuous gullies display a strong preference for the southern (polar) orientation. However, the difference from straight gullies comes from the fact that no gullies with $S > 1.10$ are found on equator-facing slopes, whereas several straight gullies are identified. Additionally, sinuous gullies occur at various latitudes, not within a fixed latitude range. For example, they do not occur only between 30° and 35°, a range of latitude for which equatorward gullies are limited in number [*Balme et al.*, 2006]. As this difference is statistically representative (25 images contain a gully with $S > 1.10$ over 250 images), it may indicate a slight but interesting difference between the orientation of straight gullies and sinuous gullies.

[12] Gullies form where steep slopes are present, with a large majority occurring on the inner walls of impact craters and occasionally on central peaks and exterior walls of impact craters [*Baker*, 2001; *Costard et al.*, 2002; *Reiss et al.*, 2009]. No systematic study of slopes was done because MOLA data are too coarse to give a precise view. Studied images indicate that sinuous gullies appear on the same parts of the hillslopes as straight gullies (as in Figures 2 and 3). Slopes where sinuous channels are observed were measured using two High Resolution Stereo Camera (HRSC) stereo pairs (Figure 6). HRSC digital elevation models (DEMs) were derived using the photogrammetric software developed by the HRSC team [*Scholten et al.*, 2005; *Gwinner et al.*, 2007]. DEMs can be locally derived down to a grid size of 30–40 m [*Ansan et al.*, 2008], but in the studied examples the texture of the surface is not favorable for such a high resolution. Since slope maps are sensitive to high-frequency noise, grids at 150 and 200 m sampling were preferred to calculate the DEMs (Figure 6). Our results indicate that sinuous channels occur on slopes between 10° and 20°. Above 20°–25°, alcoves are predominant, locally displaying straight channels on these steep slopes. Below 10° all channels vanish inside the debris fans. The sinuous channels

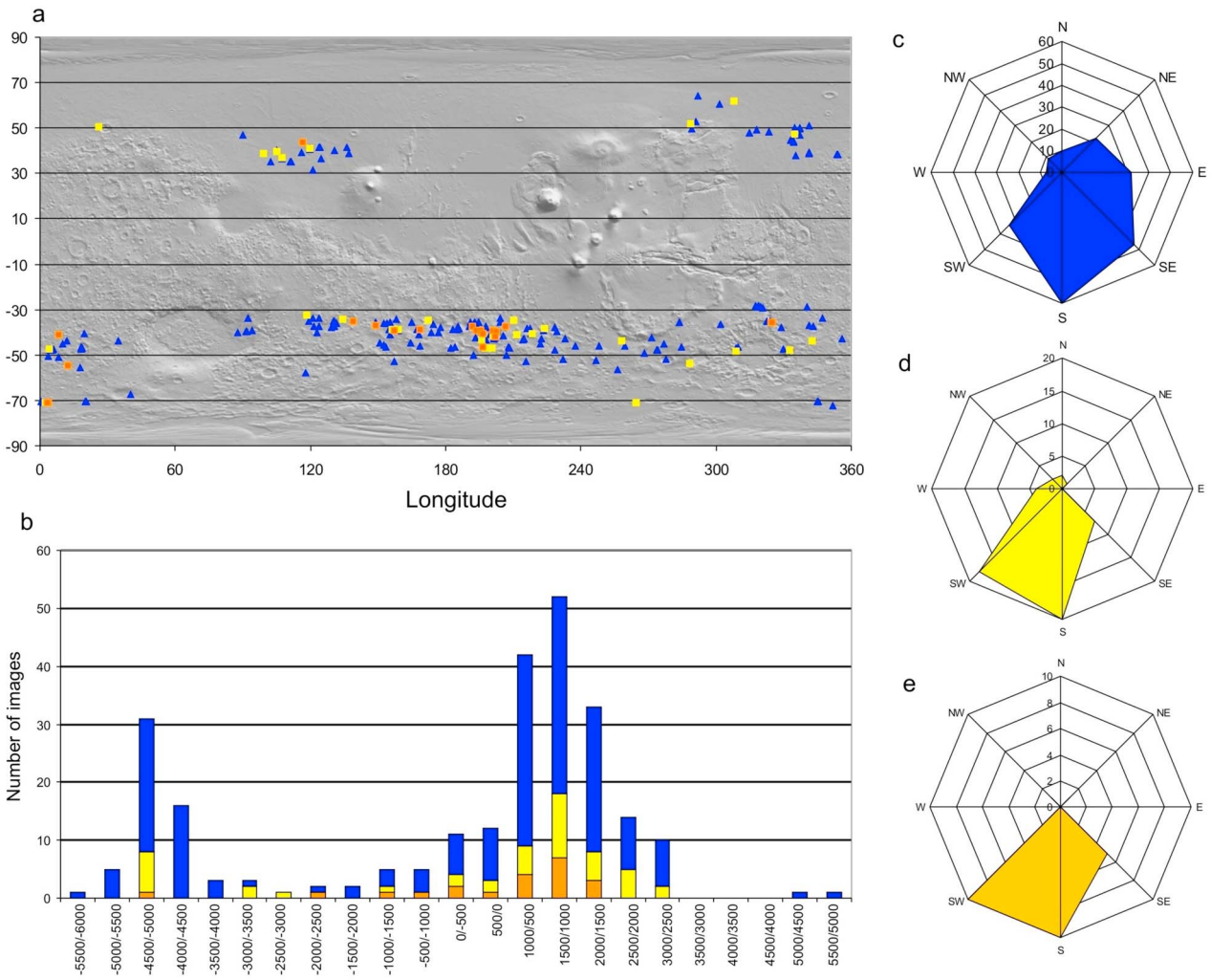

Figure 5. (a) Geographic distribution, (b) mean elevation, and (c–e) orientation of hillslopes with gullies. In blue are images with straight gullies ($S < 1.05$), in yellow are images with gently sinuous gullies with $1.05 < S < 1.10$, and in orange are highly sinuous gullies with $S > 1.10$.

visible in Figures 6f and 6i are, respectively, found on mean slopes of 14° and 12°. Straight gullies can coexist with sinuous gullies on these slopes, but they are more frequent on steeper slopes. By comparison, *Kreslavsky* [2008] measured the detailed slope variations of individual gullies using HiRISE stereo pairs finding slopes from 17° to 29°. Using HRSC DEMs, *Reiss et al.* [2009] found slopes in Hale crater gully walls from 18° to 28°. These values are consistent with the slopes at which many straight gullies are observed in our study, but they are slightly higher than those where sinuous gullies are found.

[13] In summary, sinuous gullies have distributions in elevation and latitude similar to usual (straight) gullies. An exception comes from the orientation, which may have influenced their formation on poleward-facing slopes, apparently more than the preferential orientation for straight gullies. Another difference may come from the slope, when compared to other studies, which may be slightly lower for sinuous gullies than for straight gullies. Nevertheless, it can be concluded from the similar geographic distribution that sinuous gullies do not correspond to a distinct class of gullies, and therefore they were likely formed by the same processes as usual straight gullies.

3. Interpretation in Terms of Granular Flow Dynamics

3.1. Topography Effects and Sinuosity

[14] A wide range of laboratory experiments has been performed with dry granular flows over rigid inclined planes by varying the input flux of particles and the properties of the granular material of the underlying bed (size and polydispersity of the particles, roughness, etc.). Flow instabilities such as roll waves have been observed, but to our knowledge, the generation of sinuous channels such as those observed for Martian gullies has never been obtained [e.g., *Groupement de Recherche Milieux Divisés*, 2004; *Forterre and Pouliquen*, 2003, 2008]. Fewer experimental studies of granular flows over erodible beds have been performed. Systematic studies of granular flows over thin and thick erodible substrates near the instability threshold of the granular bed have produced erosion waves when a granular

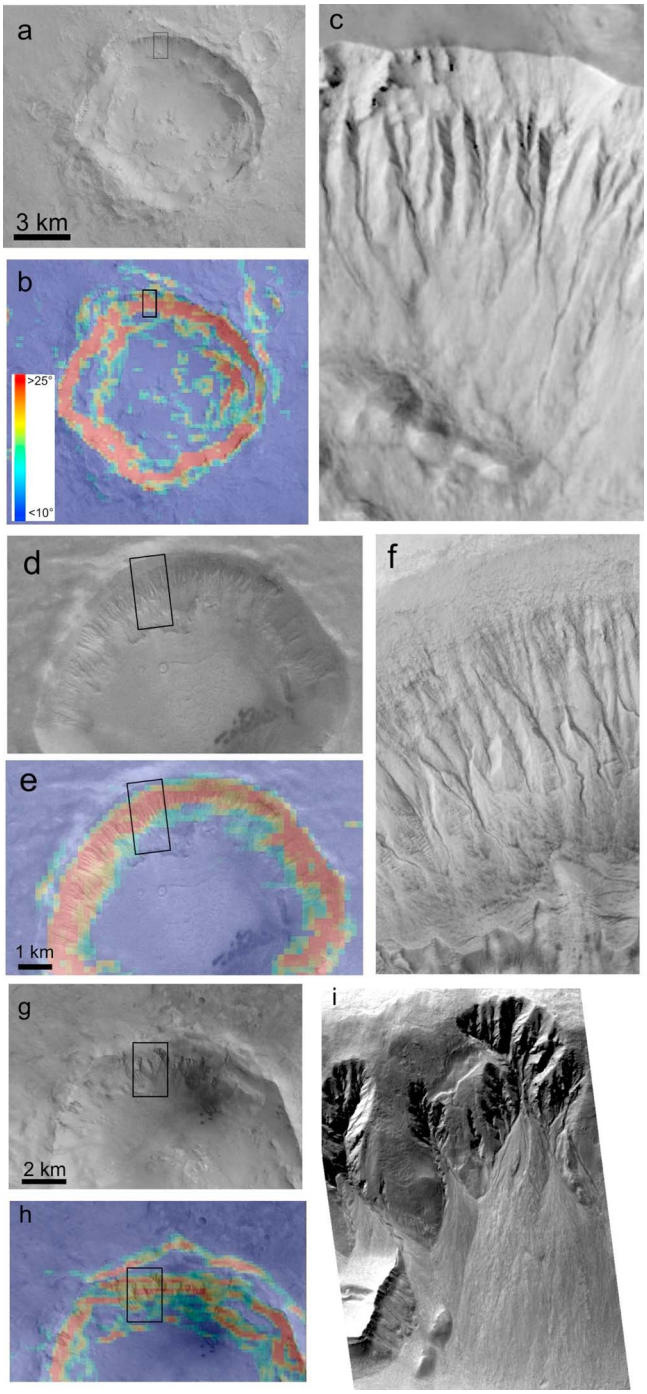

Figure 6. Close-ups of HRSC images from (a) orbit 2399 located at 35°20′S 181°40′E, (d) orbit 2399 located at 38°45′S, 181°20′E, and (g) orbit 2476 located at 38°40′S, 195°E. (b, e, and h) Corresponding HRSC slope maps with colors from blue (10° and below) to red (25° and above) and (c, f, and i) MOC close-ups of selected crater walls with the respective numbers R1002418, E1004872, and S0300928. Gullies are located in the light blue and red sections of the slope maps. Sinuous gullies, such as in Figure 6f, are visible in the slopes of 10°–20°.

mass was released on the top of the bed or when a perturbation of the free surface was imposed [*Pouliquen and Forterre*, 2002; *Maloggi et al.*, 2006; *Mangeney et al.*, 2007b]. However, no sinuous flows have been observed.

[15] On Earth, sinuosities or meandering instabilities are widely observed in natural systems at large scales (rivers) or small scales (windowpanes during a rainfall), and they are created by a variety of processes. Dry granular flows of the scale of Martian gullies can be observed on mountain debris aprons or on volcanoes in the case of pyroclastic flows. Dry granular deposits are characterized by a straight channel with narrow levees (Figure 7a) that can gently bend in response to slight topographic variations, but to our knowledge, sinuosities have not been reported. On the other hand, liquid-water-bearing debris flows on Earth have been observed to be sinuous (Figures 7b–7f). Nevertheless, the origin of sinuosities in these debris flows is unclear. In the field, variations of the local topography are often observed at scales varying from few centimeters to tens of meters (Figure 7d). These variations may play a strong role in the generation of sinuosities. In contrast, on >25° active debris aprons, such as in Figure 7a, the underlying topography is regular and may not generate enough variations to modify the flow directions. The complex behavior of self-channeling flows that create lateral static zones makes it difficult to easily assess how the flow responds to topographic oscillations [*Mangeney et al.*, 2007a]. The nonlinear interaction between flow and topography could then possibly create bends in response to changes in the steepest slope direction that can look like sinuosities for specific topography fluctuations.

[16] Martian gullies exhibit puzzling sinuosities for which a given wavelength can be defined (Figure 8a), suggesting that sinuosities result from a flow instability. Given the fact that sinuous channels are almost always observed together with straight channels, Martian flows are expected to occur in a range of conditions (slope, flux, material and bed properties) close to the potential instability threshold. Depending on flow conditions, material properties, and/or external perturbations such as topographic variations, a given flow would or would not reach the instability threshold and generate sinuosities. These conditions may be different on Mars than on Earth.

[17] The emergence of sinuosities could be possibly explained by two processes: (1) the flow could change direction in response to topographic variations or (2) flow instability could develop triggered by flow perturbation initially due to topographic variations. Thus, numerical simulations have been performed in order to test the flow response to topographic variations and in particular to assess if the complex nonlinear coupling between flow and topography may generate a sinuous instability for dry granular flows.

3.2. Looking for Sinuous Dry Granular Flows Using Numerical Modeling

[18] The numerical model used here, SHALTOP, describes granular flows over a complex three-dimensional (3D) topography [*Bouchut and Westdickenberg*, 2004; *Mangeney-Castelnau et al.*, 2005; *Mangeney et al.*, 2007a]. The model is based on the depth-averaged thin layer approximation (i.e., the flow is supposed to be thin compared to its length along the topography) and takes into account a Coulomb-type

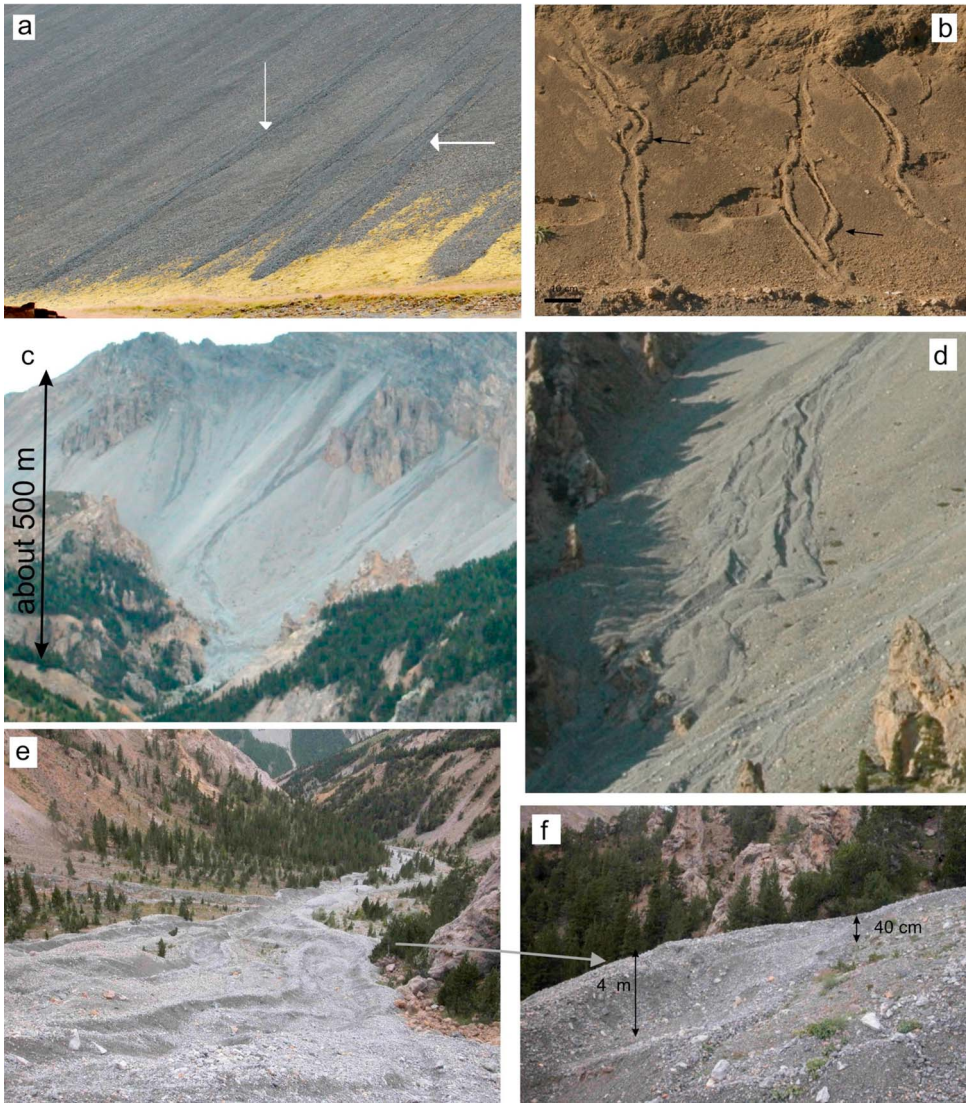

Figure 7. (a) Granular flows (arrows) over a debris apron in Iceland. Small levees are visible, and the flow is straight. (b) Examples of small leveed debris flows inside fine-grained material on 3 m high talus in the Rocky Mountains. The arrows indicate bends with asymmetric levees. Terrestrial examples of debris flows in (c) the Izoard pass in the Alps and (d and e) over a 500 m high debris apron showing local sinuosities. (f) In the bend, the external levee is thicker than the internal levee.

friction law. It describes the changes in time of the thickness $h(x, y)$ and of the depth-averaged velocity of the flow $v(x,y)$ along the topography. Contrary to most of the models used in geophysics, the model deals with the full tensor of terrain curvature that appears in momentum equations when the asymptotic development is rigorously handled. SHALTOP has been able to successfully reproduce experimental results on the spreading of small aspect ratio granular columns [*Mangeney-Castelnau et al.*, 2005] as well as natural landslides on Earth and on Mars [*Lucas and Mangeney*, 2007; *Kuo et al.*, 2009; *Lucas et al.*, 2009]. The model has been used to show that self-channeling flows over inclined beds and levees can be reproduced without taking into account the presence of water or polydispersity effects [*Mangeney et al.*, 2007a]. Actually, nonlinear coupling between a pressure gradient and a thickness-dependent friction law plays a key role in the process of levee generation. Here, we use the flow rule proposed by *Pouliquen and Forterre* [2002] for which the frictional coefficient depends on both the thickness and the velocity of the flow. The law involves four friction angles (δ_i, i = 1–4) that can be deduced from laboratory experiments and are representative of the frictional properties of the material and of the underlying bed (see *Mangeney et al.* [2007a] for more details about the flow law and the rheological parameters used in the model).

[19] The rheological parameters used here to mimic dry granular flows are characteristic of glass beads: $\delta_1 = 20°$, $\delta_2 = 32°$, $\delta_3 = 21°$, and $\delta_4 = 34°$. In general, higher friction angles are expected for natural dry granular fragments. The presence of water leads to smaller effective friction angles due to pore pressure. Indeed, in numerical models dealing with debris flows, the first-order consequence of the presence of fluid is to decrease the effective friction angle, even though viscous effects and the interaction between the fluid phase and the

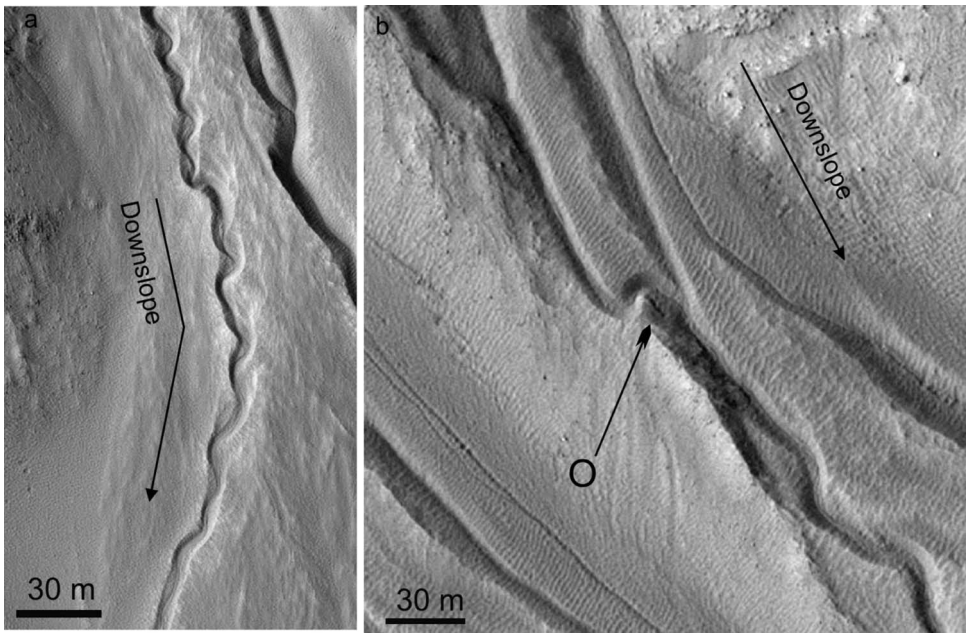

Figure 8. Two examples of sinuous gullies in HiRISE images with (a) a change in the main slope and (b) an obstacle (O) across the flow.

grains also play a significant role [*Iverson and Denlinger*, 2001; *Pelanti et al.*, 2008]. As friction angles in depth-averaged models represent the mean dissipation during the flow [*Lucas and Mangeney*, 2007], angles smaller than 20° will mimic flows that are more fluidized than granular flows, as could be the case for very small particles in the presence of air [*Roche et al.*, 2004] or when water is involved. The extreme case $\delta_i = 0°$ represents frictionless pure water flow. Note that polydispersity effects can also significantly increase the maximum distance reached by the flow, thus decreasing the effective dissipation within the flow [*Roche et al.*, 2002; *Goujon et al.*, 2007]. A wide range of plane inclination ($\theta \in [5°, 45°]$) and friction angles ($\delta_i \in [2°, 35°]$) is investigated here.

[20] A series of numerical simulations using 800×1500 grid points was performed (i.e., the space steps in the downslope x-direction and transverse y-direction are $dx = 1.8$ m and $dy = 0.3$ m, respectively). Several tests were done where granular flows were generated either by the release of a granular mass at the initial instant or by a constant flux imposed at the top of the plane, as was done for the simulation of self-channeling flows by *Mangeney et al.* [2007a]. In these simulations, sliding materials do not spontaneously display sinuous shapes when the slope is regular, whatever the initial and boundary conditions and the inclination of the plane. Furthermore, the flow always stops on slopes higher than $\theta \approx \delta_1 - 2°$, which corresponds to 18° for dry granular flow simulations.

[21] In HiRISE images we observe that several sinuous Martian gullies may have been helped by various factors such as variations in slope (as in Figure 8a) or the presence of an obstacle that modifies the trajectory of the flow (as in Figure 8b). Another parameter might be the presence of a meter-scale roughness, which is observed in several HiRISE images of depositional fans and may create the instabilities required for sinuous flows. Simulations were performed by prescribing a constant granular flux $Q_0 = 16$ m^3 s^{-1} originating from a supply with a thickness $h_0 = 1$ m, a width $w_0 = 8$ m, and an initial velocity $u_0 = 2$ m s^{-1} located at the top of the topography. Figure 9 displays simulations of dry granular flows ($\delta_1 = 20°$, $\delta_2 = 32°$, $\delta_3 = 21°$, $\delta_4 = 34°$) over a topography made of a first plane inclined at $\theta = 20°$ in the x-direction followed by a slope break toward a plane inclined at $\theta = 20°$ in the x-direction and at $\theta = 5°$ in the y-direction (Figure 9a), a topography surmounted by a parabolic obstacle of maximum thickness $h = 20$ m and extension along the plane $l = 150$ m (Figure 9b), a random rough topography with maximum roughness amplitude $A = 0.2$ m obtained using classical random number calculations (Figure 9c), and a sinusoidal fluctuation of the topography in both the longitudinal and transversal directions of wavelength $\lambda = 75$ m and amplitude increasing exponentially from $A = 0$ m on top of the plane to $A = 2$ m at 1200 m downslope (Figure 9d). These examples were chosen as representative of each studied case.

[22] A slope change of even a few degrees creates a bend in the flow (Figure 9a). The simulated granular flow has a typical thickness $h = 0.6$ m, a width $w = 130$ m, and a velocity $v = 1$ m s^{-1} before the bend and a thickness $h = 0.1$ m, a width $w = 80$ m, and a velocity $v = 1.3$ m s^{-1} after the break slope. The bend can be more or less strong depending on the flow volume, the velocity, and the difference of the slope azimuth. However, the bend never creates additional instabilities forming cyclic bends that may have resembled Martian sinuous gullies. On the contrary, the flow becomes straight again after the change of the slope, so this case can explain single bends as observed locally for some gullies, but not those observed for sinuous gullies.

[23] The presence of an obstacle thicker than the flow has a strong effect on the flow channel morphology (Figure 9b). Granular material accumulates behind the obstacle, increasing its thickness until it is wide enough to flow again, here

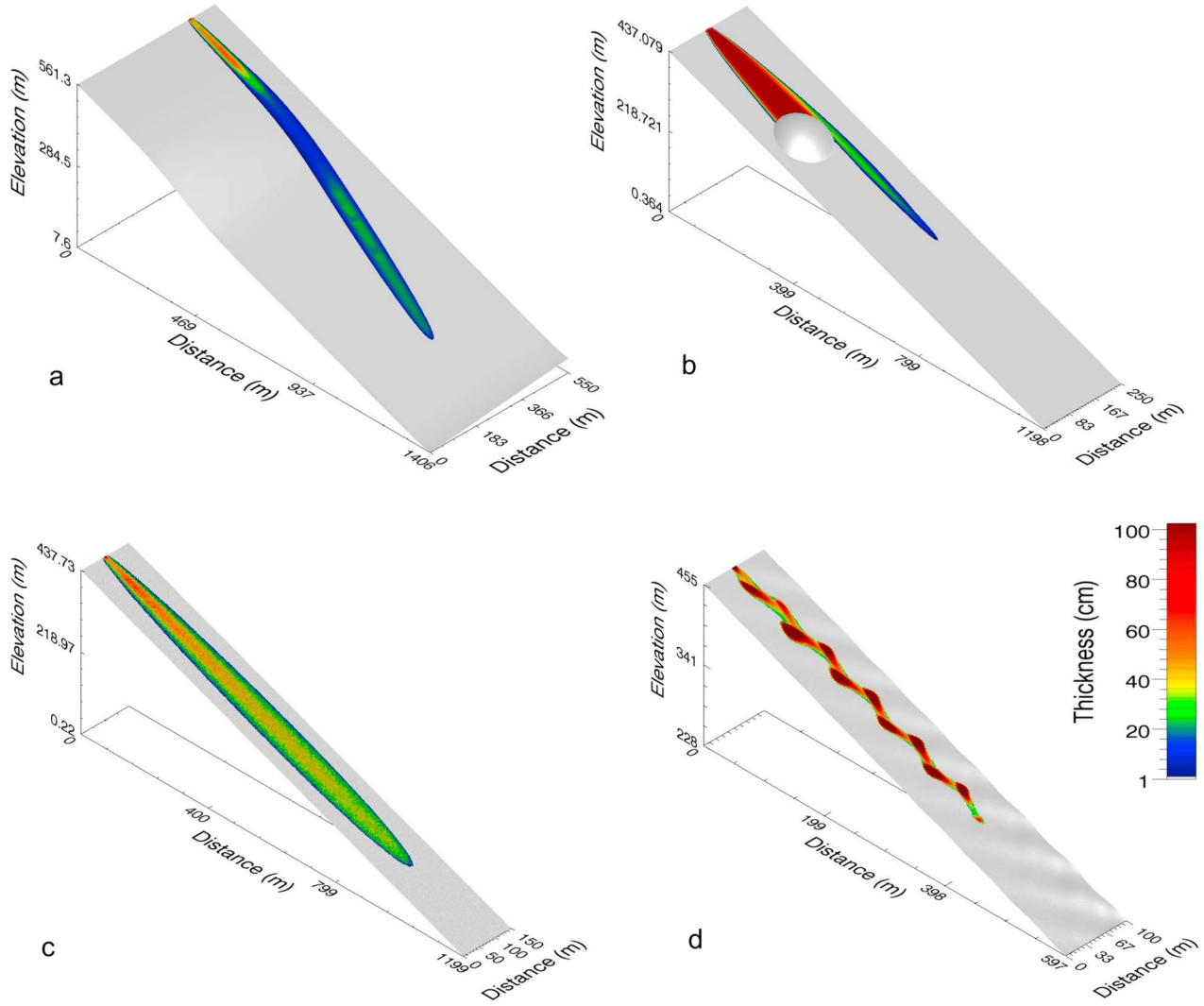

Figure 9. Numerical modeling of dry granular flows on a bed of mean inclination $\theta = 20°$ (a) with a bend in the slope, (b) with a large obstacle on the path of the flow, (c) over a 20 cm scale bedrock roughness, and (d) over a sinusoidal variation of the topography with characteristic amplitude and wavelength similar to that of the thickness and width of the flow, respectively.

on one side of the obstacle. Simulated granular flows over an obstacle have a typical thickness $h = 1.5$ m, a width $w = 180$ m, and a velocity $v = 0.6$ m s^{-1} before the obstacle and a thickness $h = 0.5$ m, a width $w = 60$ m, and a velocity $v = 0.5$ m s^{-1} after the obstacle. No sinuosity is obtained in any test with similar conditions, and again, no flow was possible on slopes smaller than $\theta \approx \delta_1 - 2°$. Furthermore, this example shows a strong difference between this type of flow and the sinuous gullies observed in Figure 8b. Indeed, in Figure 8b the obstacle modifies the direction of the flow surrounding the obstacle, but the channel width remains the same all around the obstacle, contrary to the simulated granular flow, which displays a decrease in width after the obstacle. The difference may be an effect of the cohesion and/or the viscosity of the Martian flow. Cohesion and viscosity are absent in the case of dry granular flows considered here. Cohesion may be an important parameter in Martian gullies where channel width is not modified after the obstacle, and the flow may act as a viscous cohesive body.

[24] The third test was done using a constant slope but a rough surface (Figure 9c). In that case, the typical simulated thickness, width, and velocity are $h = 0.5$ m, $w = 70$ m, and $v = 0.6$ m s^{-1}, respectively. Here, the granular flow displays strong fluctuations of its thickness, but it never tends to bend or change in direction.

[25] In the last test, the topography fluctuation has characteristic dimensions of the order of the width and thickness of the flow (Figure 9d). Thus, this test tries to maximize the possible bending of the flows to generate sinuosities. The result shows that the flow is driven by the topography variations, exhibiting sinuosities with a wavelength similar to the wavelength of the sinusoidal topography variation. Even though the mean variation of the topography is small (Figure 10), the steepest slope direction changes from downslope to transverse and makes the flow follow these

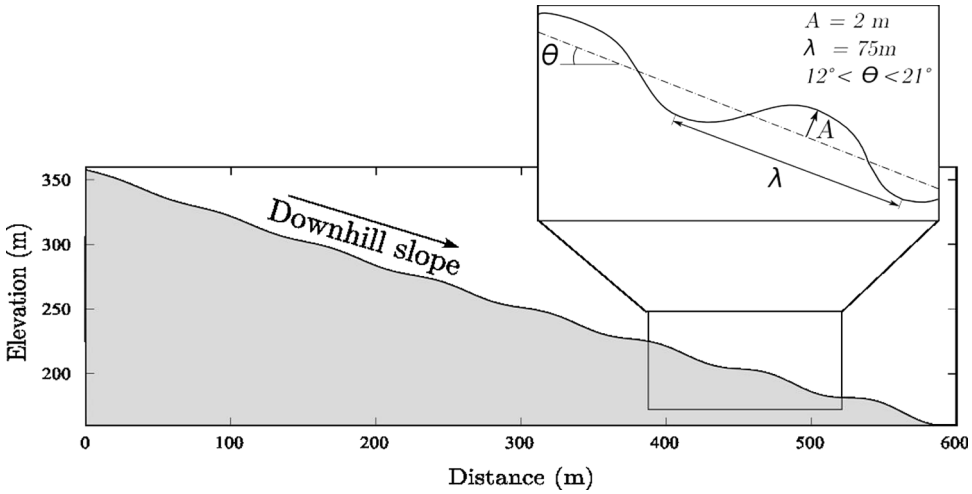

Figure 10. Downslope profile of the topography fluctuation used in the simulations. Note that the topography is uniform in the direction transverse to the slope in 3-D.

topographic variations. Here the flow generates sinuosities, but the generated flows do not replicate all Martian observations. Indeed, it was not possible to make the material flow on slopes $\theta < 18°$ such as those measured in DEMs as typically 10°–15°.

[26] As the minimum slope at which the flow occurred depends on the chosen friction angle, a series of simulations was performed with decreasing friction angles ($\delta_1 = 20°$, $\delta_1 = 15°$, $\delta_1 = 2°$). The other friction angles δ_i, $i = 2, 3, 4$, were calculated such that $\delta_i - \delta_i(\text{dry})$ is kept constant whatever i, $\delta_i(\text{dry})$ being the value of δ_i in the dry case. The topography was taken with slopes decreasing from $\delta = 21°$ to $\delta = 12°$ exponentially and with sinusoidal fluctuations similar to those used in Figure 9d (Figure 10). Figure 11 shows that the interaction between the flow and the topography is very sensitive to the friction angle of the material. As the friction angle decreases, the flow exhibits less and less sinuosity and travels farther down the plane on gentler slopes. For $\delta_1 = 20°$, the flow becomes sinuous at the very top of the plane where the amplitude of the topography variations is only of tens of centimeters and the front of the flow stops on slope $\theta = 18°$. For $\delta_1 = 15°$, the flow becomes sinuous a short distance downslope, and the mass front stops on slopes on the order of $\theta = 13°$, as observed on Mars, suggesting that the dissipation in Martian natural flows is smaller than that in dry granular flows. For $\delta_1 = 2°$, the channel is almost straight and never stops. Thus, although the material is able to flow at 10°–15° as observed for Martian gullies, the flow tends to be less sinuous, contrary to the researched effect.

[27] Our results suggest that sinuosity can be generated in dry granular flow by the topography, if topographic variations are of the same range as the flow thickness. However, even with these highly restrictive conditions, it is not possible to reproduce all gully characteristics. First, bends

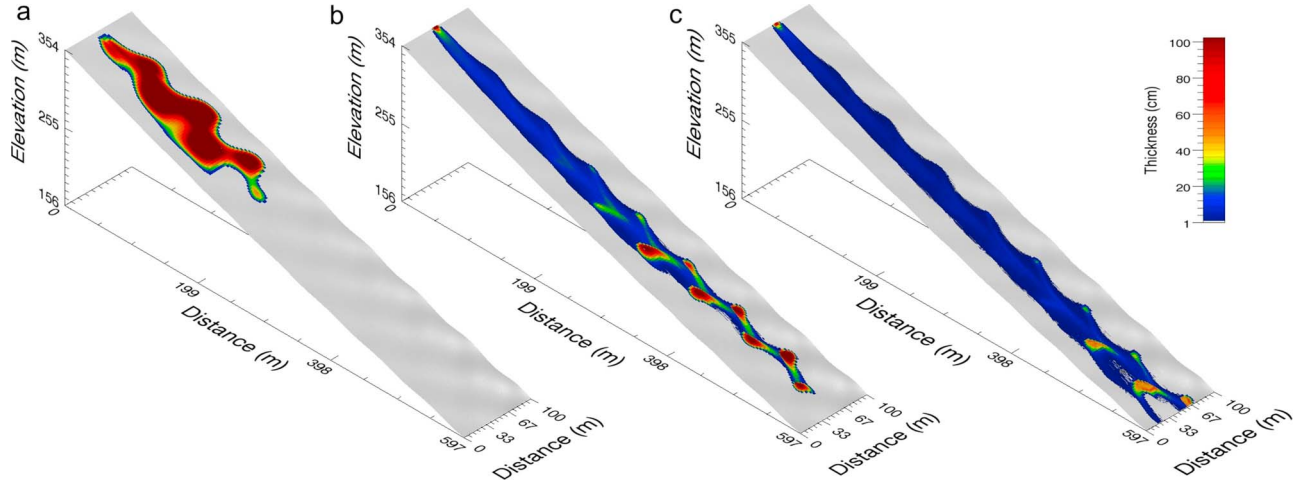

Figure 11. Numerical modeling of flows over topography with a mean slope varying from 21° on top to 12° at the bottom, with sinusoidal topography fluctuations with amplitude increasing from $A = 0$ on top of the plane to $A = 2$ m at 1200 m downslope, and with wavelength $\lambda = 75$ m for (a) dry granular flows ($\delta_1 = 20°$), (b) less dissipative flow ($\delta_1 = 15°$), and (c) almost frictionless fluid flow ($\delta_1 = 2°$).

around obstacles observed in HiRISE images (Figure 8b) are not well reproduced in simulations (Figure 9b), showing a difference in the physical parameters of the flow, such as cohesion. Second, dry granular flows are shown here to stop on slopes higher than those observed for Martian gully deposits for realistic friction angles. Third, on Mars, straight gullies are observed next to several sinuous gullies. For example, this is visible with gully B in Figure 3 and the straight gully located 30 m left of gully B. In this example it is unlikely that the apron topography may be so different so close to the sinuous flow. Therefore, topographic variations cannot fully explain the sinuosity of Martian gullies.

4. Comparison of Sinuous Gullies With Terrestrial Debris Flows

[28] Sinuous terrestrial liquid-water-bearing debris flows exist and have been described in a variety of contexts [e.g., *Johnson and Rodine*, 1984], including alpine flows inside debris aprons or arctic debris flows formed into permafrost. Some sinuous channels are visible in the terrestrial examples presented in Figures 7b–7f. The physical properties associated with these debris flows may be essential for the origin of sinuous gullies. The aim of this section is to use methods developed on Earth for these debris flows to derive physical properties such as the viscosity and velocity. The physical origin of sinuosity in terrestrial debris flows will be developed in the discussion.

4.1. Sinuous Channels in Terrestrial Debris Flows

[29] Debris flow is a term often used to describe any mass movement over a slope involving a substantial amount of liquid. In the following, we use the term "debris flow" according to its mechanical definition: fluidized material in which the proportion of solids is approximately 50%–90% by volume [e.g., *Coussot and Meunier*, 1996]. Floods and flows with less than 50% solids correspond to concentrated fluids in which solid particles are transported and deposited by the flow. Particles have no interaction except for collisions. In contrast, solid particles of debris flows are all in contact, and the whole material behaves macroscopically as a single-phase plastic fluid with cohesion [*Pierson*, 1995]. Turbulence is rare in debris flows, which are mainly laminar [e.g., *Coussot and Meunier*, 1996]. Therefore, a debris flow is a gravity-induced mass movement between landsliding and fluvial erosion, although with mechanical characteristics very different from either of these processes [*Johnson*, 1970; *Coussot and Meunier*, 1996]. The transition from hyperconcentrated flows to debris flows is marked by a rapid increase in yield strength and features indicative of plastic-fluid flow, such as lateral levees [*Pierson*, 1995]. Lateral levees are frequently observed in terrestrial debris flows (Figures 7b and 7f), but they are not ubiquitous, and their extent depends on particle grain sizes and water content. For example, water-rich mudflows may not display thick levees regardless the size of the flow. Thus, a flow larger than that in Figure 7b may not display larger levees, if composed of similar material. On Mars, gullies can display levees in MOC or HiRISE images (Figures 12a–12g), whereas many gullies also lack apparent levees (Figures 12h and 12i), but it is impossible to determine if such channels are levee-free or display too small a levee to be visible (<10 cm).

[30] Terrestrial examples show that levees in the external part of the bend are larger and thicker than the ones present in the internal part of the bend, a property that has also been observed for several Martian examples (Figures 12b–12e). The presence of levees is a critical observation for determining flow properties. In terrestrial debris flows, levees are usually visible in the lower part of the gullies, and they are often absent in the upper part, as observed in the example at Izoard pass in the French Alps (Figure 7c). The debris flows are 100–500 m long, with channels 3–15 m wide and levees from 10 cm to 4 m thick. They are initiated on debris aprons with steep slopes (>25°). Channels with levees occur at slopes between 10° and 15° as measured in situ. These debris flows form inside very rocky material where large rocks (>10 cm) predominate. Figure 10 shows a much smaller debris flow with a few 10 cm channels and 1–3 cm high levees that formed inside muddy deposits where small grain sizes predominate (<50 μm).

[31] Levees on each side of the channels are typical of flows with a yield strength [*Johnson*, 1970; *Allen*, 1997]. The yield strength corresponds to the minimum shear stress that should be applied to the material to make it flow. The Bingham flow, first proposed by *Johnson* [1970], is the simplest and most often used viscoplastic model for simulating debris flows [e.g., *Allen*, 1997]:

$$\tau = K + \mu \, \mathrm{d}\gamma/\mathrm{d}t, \text{ if } \tau > K, \tag{1}$$

where τ is the shear stress, K is the yield strength, $\mathrm{d}\gamma/\mathrm{d}t$ is the shear rate, and μ is the viscosity. If $\tau < K$, there is no internal deformation [e.g., *Allen*, 1997]. The model is relevant when yield strength is confirmed by the presence of levees. The difference in yield strength is dependent on material grain size, the density, and the water content, but not on the size of the channel. Larger initial volumes of muddy flows, with the same material as in Figure 10, would not imply larger levees.

[32] Yield strength does not vary during the flow if the material does not show changes in water content [*Coussot and Meunier*, 1996]. Therefore, at a given yield strength, the levee thickness increases when the slope decreases. The lower the slope, the higher and larger the levees are, explaining why levees are mainly visible in the lower parts of the channel. At low slope, debris flows frequently end in a terminal lobe. A change in behavior occurs when the shear stress drops below the yield strength [e.g., *Pierson*, 1995]. Such behavior can explain why gully terminal fans exist on slopes as steep as 10°.

4.2. Flow Properties of Martian Gullies From Levees and Sinuous Shapes

[33] The yield strength can be calculated from the levee thickness h and the slope α [e.g., *Johnson*, 1970; *Allen*, 1997]:

$$K = h\rho g \sin \alpha, \tag{2}$$

where g is the gravity and ρ is the fluid density. The yield strength error is directly proportional to the measurement error on the levee thickness. In the following results, we present an estimate of K from topographic information derived from photoclinometric analysis of HiRISE images

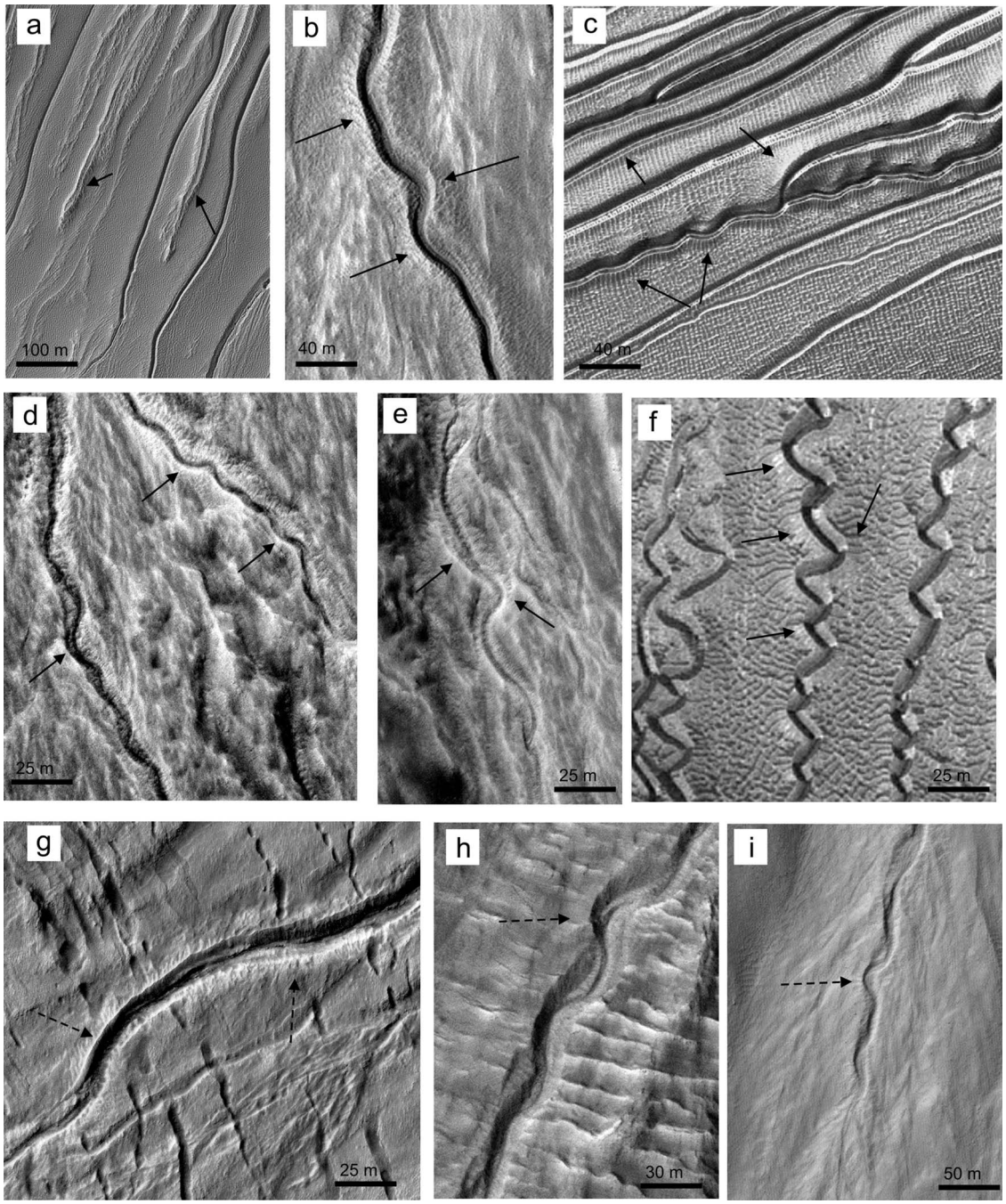

Figure 12. HiRISE image close-ups for examples of sinuous debris flows with levees of (a) PSP_1697_1390, (b) PSP_3464_1380, (c) PSP_1440_1255, (d and e) PSP_5587_1405, (f) PSP_10749_1325, (g) PSP_5943_1380, (h) PSP_12496_1410, and (i) PSP_6261_1410. Solid arrows indicate well-defined levees, and dashed arrows indicate less obvious levees.

following the method described by *Davis and Soderblom* [1984]. Models were calibrated using MOLA profiles as an envelope for topography at the scale of gullies. Results at the MOC scale were shown by *Mangold et al.* [2003] for gullies on dunes. Cross sections were chosen to be orthogonal to the flow. By assuming that the overall channel is in the direction of the main slope, orthogonal profiles should have the same elevation on both sides of the gullies, which allows us to fix the base of the small topographic profile.

[34] The method is not applicable to many of the sinuous gullies observed. Indeed, this method requires that the image intensity is uniquely due to the topography, not due to variations in surface particles' albedo. Aeolian ripples visible on many HiRISE images also modify the local topography of gully borders and aprons. Many gullies observed in HiRISE images display albedo variations that are not related only to the topography of gullies (Figures 12d–12g). Additionally, low to medium incidence angles of the Sun and a

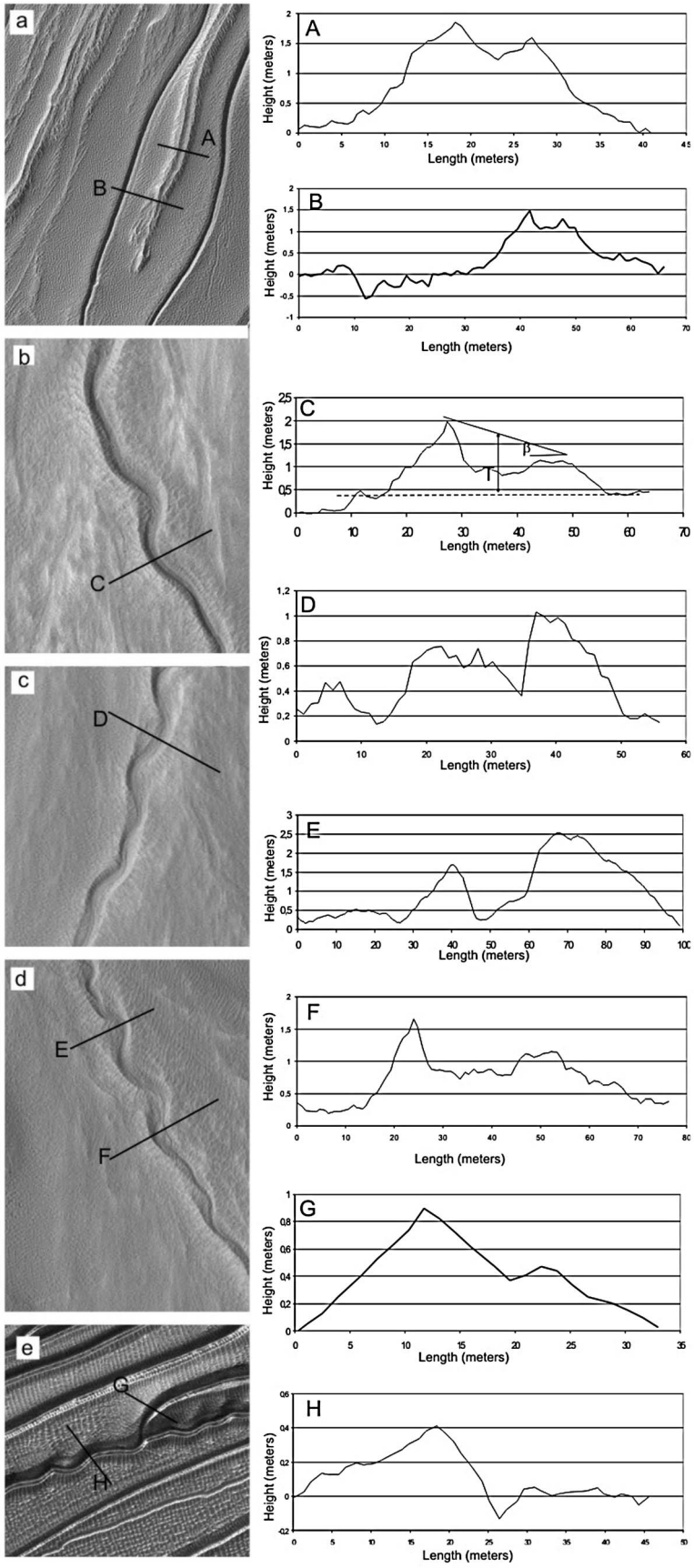

Figure 13

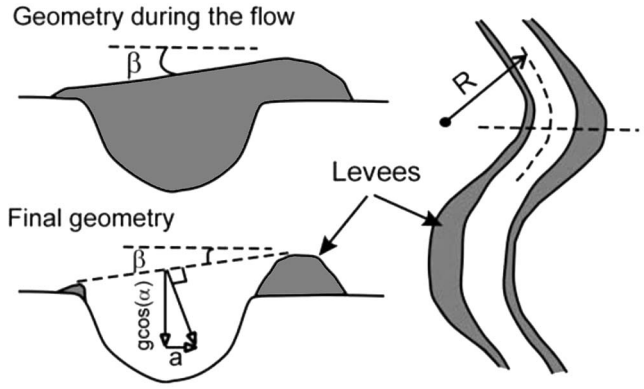

Figure 14. Schematic view of levees inside bends (right) seen from the top and (left) in cross section. The flow is tilted inside the bend, and the levees are asymmetric (adapted from *Johnson and Rodine* [1984]).

good image quality are necessary for applying this method. Finally, among the 40 HIRISE images containing gullies, photoclinometric profiles were successfully extracted for only three HiRISE images (Figure 13).

[35] Applying equation (2) to the two terrestrial examples shown in Figure 7 gives a value of approximately 100 Pa for small mudflows (Figure 7b) and approximately 10,000 Pa for rocky debris flows (Figure 7c). Results from Martian flows for the yield strength give values from a few hundred pascals to 2200 Pa. These values are in the range of terrestrial yield strengths for debris flows [e.g., *Major and Pierson*, 1992]. Notice that we estimate to approximately 10 cm the smallest levees identifiable in HiRISE images. As a consequence, materials having less than 100 Pa of yield strength could not be identified on Mars using the current data set.

[36] During the flow, velocity is usually difficult to determine without in situ measurements. Nevertheless, the asymmetry in bending levees is commonly used to determine the velocity of debris flows [*Johnson and Rodine*, 1984]. The reason for this asymmetry is that the surface of the flow tilts toward the center of curvature of the bend as a result of the radial acceleration of debris (Figure 14). The consequence of this tilt after the flow is the presence of larger and broader deposits on the outsides of channel bends. The levees are much narrower on the insides of channel bends. The method was applied to the gullies of Russell dunes [*Mangold et al.*, 2003] using MOC images, but MOC resolution constrained the results to a large uncertainty. According to *Johnson and Rodine* [1984], the mean velocity of flow inside the bends can be deduced from the radial acceleration a:

$$a = V^2/R, \tag{3}$$

where V is the velocity and R is the radius of curvature. The radial acceleration is also equal, according to Figure 14, to

$$a = g\ \cos\ \alpha\ \tan\beta, \tag{4}$$

where β is the tilt estimated from the difference of the elevation of levees (g and α as in the previous paragraph). Therefore, from equations (4) and (5),

$$V = (gR\ \cos\ \alpha\ \tan\beta)^{1/2}. \tag{5}$$

This method compares favorably with in situ measurements of velocities on Earth [*Johnson and Rodine*, 1984]. Velocities determined using this method in the two terrestrial examples give approximately 8 m s^{-1} for thick debris flows (Figure 7c) and between 1 and 2 m s^{-1} for small mudflows (Figure 7b). Results from the Martian examples give values from 1.1 to 3.3 m s^{-1} (Table 1).

[37] Viscosity μ is the most widely used parameter to characterize debris flows. The viscosity can be determined by the relationship [*Allen*, 1997]

$$\mu = (\rho g\ \sin\ \alpha)T^2/2V. \tag{6}$$

All parameters are known except the channel thickness, T, which can also be measured by photoclinometric profiles (see Figure 13c). Using this method, the two terrestrial flows are estimated at approximately 2 Pa s for the small mudflows in Figure 7b and at 1500 Pa s for the thick debris flows in Figure 7c. The viscosity of the Martian examples (Figure 15) obtained is from 40 to 1040 Pa s.

[38] Uncertainties in these calculations are dominated by errors in photoclinometric profiles, which are large but difficult to estimate without better knowledge of the true topography. In this situation, measurements made using two sections of the same gullies (examples in A and B or E and F) are seen as the best estimation for an order of magnitude of the uncertainties, which correspond to about a factor of 2 for the velocity, with the error for the viscosity being probably larger.

[39] Velocities are among the range found for terrestrial debris flows, for the two examples in Figures 7b and 7c and from a compilation of data from *Corominas et al.* [1996]. In this compilation, terrestrial debris flows from around the world were measured at velocities from 1 to 12 m s^{-1}, with varying water content. Velocities appear slightly higher for Russell crater dune gullies (profiles G and H) than for more classic gullies (profiles C–F).

[40] Figure 15 compares the viscosity of terrestrial debris flows and experimental slurries to our results. Martian viscosities are in the range of terrestrial debris flows. Terrestrial and experimental data show an increase in viscosity with the increase in the solid fraction. Assuming that Martian flows contain liquid water, the plot suggests that they contain a relatively low proportion of water (<40%). For Russell crater dune gullies (cases G–H in Figure 13) our measurements confirmed and improved the rough estimates of *Mangold et al.* [2003] done at MOC scale, in which velocity was estimated in the range 1.1–7.3 m s^{-1} and viscosity was estimated from 1 to 10^5 Pa s. Lower values found for these dune gullies with regard to the other examples studied may correspond to either a higher fraction of water (such as 40%–50%) or, alternatively, to the abundance of fine-grained

Figure 13. Photoclinometric profiles of three HiRISE image close-ups of (a) PSP_1697_1390, (b–d) PSP_3464_1380, and (e) PSP_1440_1255. Profiles on the right (A–H) are photoclinometric profiles corresponding to the respective topographic sections in Figures 13a–13e.

Table 1. Physical Properties of Gullies Using Profiles in Figure 13

Profile	Yield Strength, K (Pa)	Velocity, V (m s^{-1})	Viscosity, μ (Pa s)
A	2200	–	–
B	<120	–	–
C	1800	2.0	460
D	840	1.9	1040
E	1900	1.1	290
F	1100	1.7	450
G	840	3.3	95
H	380	2.6	40

material that can reduce viscosity without requiring more liquid water in the mixture. Viscosities found for these flows from tens to hundreds of Pa.s are comparable to those of the most fluid volcanic lava flows in Hawaii [e.g., *Nichols*, 1939].

5. Discussion

5.1. Control Parameters for the Sinuosity Threshold

[41] The origins of sinuous shapes in liquid-water-bearing debris flows are not well-known. No terrestrial study has explained the development of this type of channel in debris flows, despite the fact that observations exist and are used to determine velocities. Laboratory experiments are mainly performed along straight flumes [e.g., *Iverson*, 1997] where sinuosities are limited by channel width.

[42] In dry granular numerical modeling, the only way found to simulate sinuosity has been to impose small topographic variations at the scale of the thickness and width of the flow. In that case, simulated flows are deflected and produce sinuous shapes that can look like those of natural debris flows. As topography fluctuations investigated here are small and may be hardly visible in satellite imagery, our simulations suggest being very careful when analyzing sinuous shapes in terms of mechanical behavior of the flow. DEMs at submeter scale are required for a better analysis. Nevertheless, for the sinuous bends to occur on slopes $10° < \theta < 20°$ (as observed for Martian sinuous gullies), the effective friction coefficient has to be smaller than the values typical of dry granular materials. Such small values may be related to the presence of a fluid phase that can be gas in the case of small particles ($d < 100$ μm [*Roche et al.* 2004]), or a fluid such as liquid water for larger particles like those expected to be involved in the gullies studied here. Furthermore, the example in Figure 9b shows how granular flows are disrupted by an obstacle in a way different from the observation of Martian gullies (Figure 8b). Therefore, the cohesion of the flow seems to be a necessary characteristic to generate the sinuous shapes observed.

[43] Although gullies are observed over granular debris aprons, the flowing mass may erode the initially static material. Recently, it has been shown that the entrainment of debris located on debris flow paths can generate instabilities such as surges and is a key ingredient of debris flow dynamics [*Mangeney et al.*, 2007a, 2010]. Such a process is poorly taken into account in current numerical models and may be a potential ingredient in the generation of sinuous shapes. That possibility is still to be tested.

[44] Terrestrial rivers display various regimes in alluvial plains depending on discharge rates, with (1) straight channels at low discharge rates, then (2) meandering streams, and then (3) braiding at high discharge rates [e.g., *Knighton*, 1998]. Similar regimes are obtained by *Le Grand-Piteira et al.* [2006] for experimental meter-scale sinuous streams (rivulets) of water flowing down a rigid substrate. They show that, for increasing flow rates, three main regimes are observed: (1) straight rivulets along the steepest slope, (2) meandering rivulets (above a critical flow rate the straight stream is unstable and perturbations of the flow lead to stationary sinuous streams), and (3) a dynamic regime where meanders no longer remain stable and vary like braids. Experiments of *Le Grand-Piteira et al.* [2006] show that the instability threshold increases with decreasing slope angle. As a result, when the slope decreases while the discharge rate remains the same, the flow may still be unable to develop sinuosities. Observation of similar regimes for very different flow types suggests that this condition may exist for other flows. Several observations of Martian gullies are consistent with the different regimes described. Indeed, downstream of sinuous gullies where the slope decreases, channels are frequently straight (examples in Figures 2 and 3 display straight channels at the termination of the flow). Although braided flows are locally observed at the HiRISE scale [e.g., *McEwen et al.*, 2007], and are frequently found on steep slopes, they seem nevertheless to occur at any location of the flow. Further work would then be needed to confirm this comparison. Nevertheless, if this similarity in flow regimes exists, then it would suggest that sinuous debris flows follow laws analogous to liquid water flows,

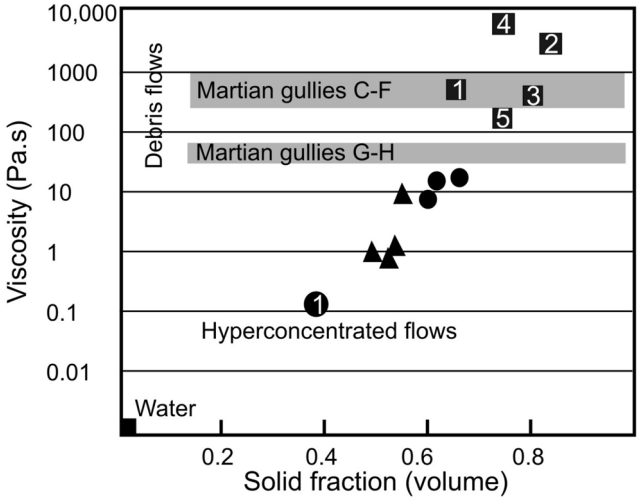

Figure 15. Viscosity versus solid fraction for terrestrial and experimental slurries and for Martian gullies. In situ measurement compilation from *Corominas et al.* [1996] (numbered squares): (1) Mt. Thomas, New Zealand [*Pierson*, 1981] for both debris flows and hyperconcentrated flows; (2) Tenmile Range, Colorado [*Curry*, 1966]; (3) Jiang Jia, China [*Li et al.*, 1983]; (4) Wrightwood-1973, California [*Morton and Campbell*, 1974]; (5) Wrightwood-1941 [*Sharp and Nobles*, 1953]. Experimental data from *Major and Pierson* [1992] for a mixture of sand and fines, with the sand dominating (circles) or with the fines dominating (triangles). Letters for Martian gullies C–F and G–H correspond to examples in Figure 13 for which the viscosities are compiled in Table 1.

but with different instability thresholds and different physical mechanisms.

[45] Further work must be performed on both terrestrial and Martian sinuous debris flows to investigate the role of cohesion, erosion, or fluid/solid mixture behavior in sinuosity instability. This is a very difficult issue because of the scaling problems between experimental and natural debris flows [*Iverson*, 1997; *Iverson and Denlinger*, 2001; *Védie et al.*, 2008] and because of the mathematical and numerical difficulties related to mixture models and to the description of erosion processes [*Pelanti et al.*, 2008; *Bouchut et al.*, 2008; *Fernandez-Nieto et al.*, 2008; *Mangeney et al.*, 2007b]. Our next step in that direction will be to use a numerical model of liquid-water-bearing debris flows to simulate sinuosities using tests similar to those performed in the present work.

5.2. Presence or Absence of Levees: Could River Streams Explain the Observations?

[46] In this study, we showed that levees seen in HiRISE imagery consist of microlandforms that are key to understanding the physical properties of flows. However, in HiRISE images, levees are often difficult to identify, are limited in size, or are absent. The presence of levees as part of the flow on steep slopes (>10°) certifies the channel origin by a debris flow with a defined yield strength, because other type of levees formed by rivers are due to deposition in low-energy environments. However, the absence of visible levees does not certify that flows were not formed as debris flows. Materials with levees of <10 cm (approximately < 100 Pa of yield strength on a 10° slope) likely cannot be identified with HiRISE imagery. Debris flows containing fine-grained material (such as clay-size grains) or a high proportion of water (30%–50%) can behave as a debris flow, but with a yield strength between 1 and 100 Pa, as the small mud flows observed in Figure 7b, or as shown by the experimental data for viscous clay-rich slurries [*Major and Pierson*, 1992]. These sorts of clay-rich/silt-rich debris flows are likely present on Mars due to the abundance of aeolian particles such as dust and silt grains [e.g., *Védie et al.*, 2008], and therefore, they may explain part of the apparent lack of levees in flows that would still correspond to debris flows.

[47] Alternatively, the lack of levees could mean that the flow is not a debris flow (defined as a viscous fluid with a given yield strength). Several studies have proposed that Martian gullies are formed from river-like activity [e.g., *Levy et al.*, 2009]. Pure liquid flows, (e.g., clear-water streams) are known to generate sinuosity, usually called meanders when $S > 1.2$. However, all meandering rivers are observed at slopes of 1°–2° [e.g., *Knighton*, 1998]. No river is known to display the sinuosity of $S = 1.2$ that has been observed for several gullies on slopes as steep as 15°. Furthermore, meanders are the result of an evolution, from a slight curve to a meander, with progressive erosion of the external bank [e.g., *Knighton*, 1998]. The observed gullies (such as in Figure 3) do not show an evolution from a straight channel to a sinuous channel. Though we can exclude pure water stream activity for nonleveed sinuous flows, hyperconcentrated flows (with typically >30% solid particles) may be a plausible process. Indeed, these flows often follow an intermediate state between turbulent stream flows and laminar viscous debris flows [e.g., *Allen*, 1997]. Whether hyperconcentrated flows explain part of the sinuous nonleveed flows, they would be less viscous than sinuous leveed flows, as a consequence of a higher proportion of liquid water or of higher fine grain content. The presence of levees would then correspond to upper bounds for the viscosity of sinuous flows.

5.3. Consequences of the Lack of Equator-Facing Slopes in Sinuous Gullies

[48] Most sinuous gullies occur in locations (latitudes, elevations, and slopes) that are similar to those of straight gullies. Nevertheless, we have observed that sinuous gullies are found only in pole-facing slopes, independent of the latitude at which they are found. Such a difference may be due to a different flow rheology such as a higher viscosity or lower water content for equator-facing gullies. Indeed, if pole-facing gullies are due to debris flows bearing water, or even hyperconcentrated flows when displaying no levee, the straight equator-facing slopes may then correspond to more viscous flows. The difference may also be due to a stronger difference in the process of formation. Indeed, morphologic parameters found in granular flow models are in the same range of values as those observed for Martian gullies. Thus, straight dry gullies can display properties similar to those of straight liquid-water-bearing gullies. Therefore, we do not exclude the possibility that some sparsely gullied crater walls present on equator-facing slopes, where sinuous channels are absent, were formed by dry flows instead of wet flows.

[49] The presence of sinuous gullies in pole-facing slopes is interesting with regard to models explaining gully formation by near-surface ice/snow melting. In *Costard et al.* [2002], modeling conditions of gully formation imply a preferential orientation toward the poles resulting from a formation at high obliquity, since the insolation on pole-facing slopes considerably increases as soon as the obliquity reaches values around 35°. Qualitatively, equator-facing slopes do not warm up in the 30°–40° latitude regions, because they are not illuminated by the Sun for enough time, whereas pole-facing slopes are warmed all day at these latitudes. The presence of sinuous gullies on pole-facing slopes only suggests more wet debris flows on these orientations than on equator-facing slopes, as predicted by the model.

6. Conclusions

[50] Our study questions the role of granular flows in Martian gully formation by focusing on the sinuous shapes observed for many recent Martian gullies. First, we have shown using 250 Mars Orbiter Camera images that sinuous gullies present a sinuosity index up to 1.25, but that only 3.5% of individual gullies display an index > 1.05 indicating a sinuous shape. They are found in locations and on slopes similar to those of straight gullies and are, therefore, related to the same formation processes. The lack of well-developed sinuous gullies on equator-facing slopes suggests a reduced role for liquid water.

[51] Second, simulations of granular flows were performed invoking potential instability triggers such as obstacles, roughness, or slope change in order to generate bends in the flow, but most simulations failed to reproduce sinuous shapes. Sinuous shapes are only simulated when grains flow

over a surface artificially containing periodic topographic variations with amplitude and wavelength comparable to the thickness and width of the channel, repectively. Nevertheless, the required friction angles to produce sinuous shapes at slopes about 10°–20° are so low that they imply the presence of an additional fluid phase in the flow. Moreover, simulations with an obstacle on the flow pathway show a strong difference in behavior with the Martian observation, where the cohesion of the flow seems to be an important parameter. Given these results and the presence of sinuous flows in natural terrestrial debris flows involving water, we have concluded that Martian gullies are better reproduced by liquid-water-bearing debris flows or perhaps hyperconcentrated flows. The physical processes behind the formation of the sinuous shape are still poorly known, but we suggest that material entrainment and cohesion may play a key role in the sinuous channels' formation. These factors need to be explored.

[52] Third, we used the presence of bends in leveed flows to extract the mechanical parameters of several Martian gullies. We obtained values for yield strength of 100–2200 Pa, velocities of 1.1–3.3 m s^{-1}, and viscosities from 40 to 1040 Pa s, which are inside the range of values for terrestrial debris flows with various proportions of liquid water. Therefore, our work confirms previous interpretations favoring most of the gully formation by liquid-water-bearing debris flows. A numerical model for liquid-water-bearing debris flows is under development, and simulations will be presented in future studies.

[53] **Acknowledgments.** The authors appreciate comments by R. Irwin and an anonymous reviewer. The authors acknowledge the use of Mars Orbiter Camera images processed by Malin Space Science Systems, available at http://www.msss.com/moc_gallery/, and images from the HRSC Experiment Team of the German Aerospace Center (DLR) Berlin. We acknowledge the efforts of the HRSC experiment technical teams and coinvestigators. This work was supported by the ANR (Agence Nationale pour la Recherche) under the program entitled PLANETEROS (under BLAN06-1_140039) and by the French Space Agency (CNES).

References

Allen, P. A. (1997), *Earth Surface Processes*, 404 pp., Blackwell Sci., Malden, Mass.

Ansan, V., N. Mangold, P. Masson, E. Gailhardis, and G. Neukum (2008), Topography of valley networks on Mars from Mars Express High Resolution Stereo Camera digital elevation models, *J. Geophys. Res.*, *113*, E07006, doi:10.1029/2007JE002986.

Baker, V. R. (2001), Water and the Martian landscape, *Nature*, *412*, 228–237.

Balme, M., N. Mangold, D. Baratoux, F. Costard, M. Gosselin, P. Masson, P. Pinet, and G. Neukum (2006), Orientation and distribution of recent gullies in the southern hemisphere of Mars: Observations from High Resolution Stereo Camera/Mars Express (HRSC/MEX) and Mars Orbiter Camera/Mars Global Surveyor data, *J. Geophys. Res.*, *111*, E05001, doi:10.1029/2005JE002607.

Berman, D. C., W. K. Hartmann, D. A. Crown, and V. R. Baker (2005), The role of arcuate ridges and gullies in the degradation of craters in the Newton Basin region of Mars, *Icarus*, *178*, 465–486.

Bouchut, F., and M. Westdickenberg (2004), Gravity driven shallow water models for arbitrary topography, *Commun. Math. Sci.*, *2*, 359–389.

Bouchut, F., E. D. Fernandez-Nieto, A. Mangeney, and P.-Y. Lagrée (2008), On new erosion models of Savage-Hutter type for avalanches, *Acta Mech.*, *199*, 181–208, doi:10.1007/s00707-007-0534-9.

Bridges, N. T., and C. N. Lackner (2005), Age-orientation relationships of northern hemisphere Martian gullies and "pasted-on" mantling unit: Implications for near surface water migration in Mars' recent history, *Lunar Planet. Sci.* [CD-ROM], *XXXVI*, Abstract 1764.

Christensen, P. (2003), Formation of recent Martian gullies through melting of extensive water-rich snow deposits, *Nature*, *422*, 45–48.

Corominas, J., J. Remondo, P. Farias, M. Estevao, J. Zezere, J. Dias de Teran, R. Dikau, L. Schrott, J. Moya, and A. Gonzalez (1996), Debris flow, in *Landslide Recognition: Identification, Movement and Causes*, edited by R. Dikau et al., pp. 161–180, John Wiley, New York.

Costard, F., F. Forget, N. Mangold, and J. P. Peulvast (2002), Formation of recent Martian debris flows by melting of near-surface ground ice at high obliquity, *Science*, *295*, 110–113.

Coussot, P., and M. Meunier (1996), Recognition, classification and mechanical description of debris flows, *Earth Sci. Rev.*, *40*, 209–227.

Curry, R. R. (1966), Observation of alpine mudflows in the Tenmile range, central Colorado, *Geol. Soc. Am. Bull.*, *77*, 771–776.

Davis, P. A., and L. A. Soderblom (1984), Modeling crater topography and albedo from monoscopic Viking Orbiter images: 1. Methodology, *J. Geophys. Res.*, *89*(B11), 9449–9457.

Felix, G., and N. Thomas (2004), Relation between dry granular flow regimes and morphology of deposits: Formation of levees in pyroclastic deposits, *Earth Planet. Sci. Lett.*, *221*, 197–213.

Fernandez-Nieto, E., F. Bouchut, D. Bresch, M. J. Castro-Diaz, and A. Mangeney (2008), A new Savage-Hutter type model for submarine avalanches and generated tsunami, *J. Comput. Phys.*, *227*(16), 7720–7754.

Forterre, Y., and O. Pouliquen (2003), Long-surface-wave instability in dense granular flows, *J. Fluid Mech.*, *486*, 21–50.

Forterre, Y., and O. Pouliquen (2008), Flows of dense granular media, *Annu. Rev. Fluid Mech.*, *40*, 1–24.

Goujon, C., B. Dalloz-Dubrujeaud, and N. Thomas (2007), Bidisperse granular avalanches on inclined planes: A rich variety of behaviors, *Eur. Phys. J. E*, *23*, 199–215.

Groupement de Recherche Milieux Divisés (2004), On dense granular flows, *Eur. Phys. J. E*, *14*, 341–365.

Gwinner, K., F. Scholten, R. Jaumann, T. Roatsch, J. Oberst, and G. Neukum (2007), Global mapping of Mars by systematic derivation of Mars Express HRSC high-resolution digital elevation models and orthoimages, paper presented at Extraterrestrial Mapping Workshop on Advances in Planetary Mapping, ISPRS Comm. IV, Working Group 9, Houston, Tex.

Haberle, B., C. P. McKay, J. Schaeffer, N. Cabrol, E. A. Grin, A. P. Zent, and R. Quinn (2001), On the possibility of liquid water on present-day Mars, *J. Geophys. Res.*, *106*, 23,317–23,326.

Heldmann, J. L., and M. T. Mellon (2004), Observations of Martian gullies and constraints on potential formation mechanisms, *Icarus*, *168*, 285–304.

Hoffman, N., L. P. Knauth, S. Klonowski, D. Burt, R. S. Saunders, R. W. Zurek, P. T. Doran, and S. L. Forman (2000), Ideas about the surface runoff features on Mars, *Science*, *290*, 711–714.

Ingersoll, A. P. (1970), Mars: Occurrence of liquid water, *Science*, *168*, 972–973.

Ishii, T., and S. Sasaki (2004), Formation of recent Martian gullies by avalanches of CO_2 frost, *Lunar Planet. Sci.* [CD-ROM], *XXXV*, Abstract 1556.

Iverson, R. M. (1997), The physics of debris flows, *Rev. Geophys.*, *35*, 245–296.

Iverson, R. M., and R. P. Denlinger (2001), Flow of variably fluidized granular masses across three-dimensional terrain: 1. Coulomb mixture theory, *J. Geophys. Res.*, *106*, 537–552.

Johnson, A. M. (1970), *Physical Processes in Geology*, 576 pp., W. H. Freeman, New York.

Johnson, A. M., and J. R. Rodine (1984), Debris flow, in *Slope Instability*, edited by D. Brundsen and D. B. Prior, pp. 257–361, John Wiley, New York.

Knighton, D. (1998), *Fluvial Forms and Processes: A New Perspective*, 383 pp., Oxford Univ. Press, New York.

Kreslavsky, M. A. (2008), Slope steepness of channels and aprons: implications for origin of Martian gullies, in *Workshop on Martian Gullies: Theories and Tests, February 4–5, Houston, Texas*, *LPI Contrib.*, 1301, Abstract 8034.

Kuo, C. Y., Y. C. Tai, F. Bouchut, A. Mangeney, M. Pelanti, R. F. Chen, and K. J. Chang (2009), Simulation of Tsaoling landslide, Taiwan, based on Saint Venant equations over general topography, *Eng. Geol.*, *104*(3–4), 181–189.

Le Grand-Piteira, N., A. Daerr, and L. Limat (2006), Meandering rivulets on a plane: A simple balance between inertia and capillarity, *Phys. Rev. Lett.*, *96*, 254503, doi:10.1103/PhysRevLett.96.254503.

Levy, J. S., J. W. Head, D. R. Marchant, J. L. Dickson, and G. A. Morgan (2009), Geologically recent gully-polygon relationships on Mars: Insights from the Antarctic Dry Valleys on the roles of permafrost, microclimates, and water sources for surface flow, *Icarus*, *201*, 113–126.

Li, J., Y. Yuan, C. Bi, and D. Luo (1983), The main features of the mudflow in Jiang-Jia ravine, *Z. Geomorphol.*, *27*, 325–341.

Lucas, A., and A. Mangeney (2007), Mobility and topographic effects for large Valles Marineris landslides on Mars, *Geophys. Res. Lett.*, *34*, L10201, doi:10.1029/2007GL029835.

Lucas, A., A. Mangeney, D. Mège, and F. Bouchut (2009), Landslide scar geometry effect on flow spreading: Application to Martian landslides, *Lunar Planet. Sci.*, *XL*, Abstract 1770.

Major, J. J., and T. C. Pierson (1992), Debris flow rheology: Experimental analysis of fine-grained slurries, *Water Resour. Res.*, *28*, 841–857.

Malin, M. C., and K. S. Edgett (2000), Evidence for recent groundwater seepage and surface runoff on Mars, *Science*, *288*, 2330–2335.

Malin, M. C., and K. S. Edgett (2001), Mars Global Surveyor Mars Orbiter Camera: Interplanetary cruise through primary mission, *J. Geophys. Res.*, *106*, 23,429–23,570.

Mallogi, F., J. Lanuza, B. Andreotti, and E. Clement (2006), Erosion waves: Transverse instabilities and fingering, *Europhys. Lett.*, *75*, 825.

Mangeney, A., F. Bouchut, N. Thomas, J. P. Vilotte, and M. O. Bristeau (2007a), Numerical modeling of self-channeling granular flows and of their levee-channel deposits *J. Geophys. Res.*, *112*, F02017, doi:10.1029/2006JF000469.

Mangeney, A., L. S. Tsimring, D. Volfson, I. S. Aranson, and F. Bouchut (2007b), Avalanche mobility induced by the presence of an erodible bed and associated entrainment, *Geophys. Res. Lett.*, *34*, L22401, doi:10.1029/2007GL031348.

Mangeney, A., O. Roche, O. Hungr, N. Mangold, G. Faccanoni, and A. Lucas (2010), Erosion and mobility in granular collapse over sloping beds, *J. Geophys. Res.*, *115*, F03040, doi:10.1029/2009JF001462.

Mangeney-Castelnau, A., B. Bouchut, J. P. Vilotte, E. Lajeunesse, A. Aubertin, and M. Pirulli (2005), On the use of Saint Venant equations for simulating the spreading of a granular mass, *J. Geophys. Res.*, *110*, B09103, doi:10.1029/2004JB003161.

Mangold, N., F. Costard, and F. Forget (2003), Debris flows over sand dunes on Mars: Evidence for liquid water, *J. Geophys. Res.*, *108*(E4), 5027, doi:10.1029/2002JE001958.

McEwen, A. S., et al. (2007), Mars Reconnaissance Orbiter's High Resolution Imaging Science Experiment (HiRISE), *J. Geophys. Res.*, *112*, E05S02, doi:10.1029/2005JE002605.

Mellon, M. T., and R. J. Phillips (2001), Recent gullies on Mars and the source of liquid water, *J. Geophys. Res.*, *106*(E10), 23,165–23,180.

Miliken, R. E., J. F. Mustard, and D. L. Goldsby (2003), Viscous flow features on the surface of Mars: Observation from high-resolution Mars Orbiter Camera (MOC) images, *J. Geophys. Res.*, *108*(E6), 5057, doi:10.1029/2002JE002005.

Morton, D. M., and R. H. Campbell (1974), Spring mudflows at Wrightwood, S. California, *Q. J. Eng. Geol.*, *7*, 377–384.

Musselwhite, D. S., T. D. Swindle, and J. Lunine (2001), Liquid CO_2 breakout and the formation of recent small channels on Mars, *Geophys. Res. Lett.*, *28*, 1283–1285.

Nichols, R. (1939), Viscosity of lava, *J. Geol.*, *47*, 290–302.

Pelanti, M., F. Bouchut, and A. Mangeney (2008), A Roe-type scheme for two-phase shallow granular flows over variable topography, *Math. Modell. Numer. Anal.*, *42*, 851–885.

Pierson, T. C. (1981), Dominant particle support mechanisms in debris flows at Mt. Thomas, New Zealand, and implications for flow mobility, *Sedimentology*, *28*, 49–60.

Pierson, T. C. (1995), Flow characteristics of large eruption-triggered debris flows at snow-clad volcanoes: Constraints for debris flow models, *J. Volcanol. Geotherm. Res.*, *66*, 283–294.

Pouliquen, O., and Y. Forterre (2002), Friction law for dense granular flows: Application to the motion of a mass down a rough inclined plane, *J. Fluid Mech.*, *453*, 133–151.

Reiss, D., H. Hiesinger, E. Hauber and K. Gwinner (2009), Regional differences in gully occurrence on Mars: A comparison between the Hale and Bond craters, *Planet. Space Sci.*, *57*, 958–974.

Roche, O., M. A. Gilbertson, J. C. Phillips, and R. S. J. Sparks (2002), Experiments on deaerating granular flows and implications for pyroclastic flow mobility, *Geophys. Res. Lett.*, *29*(16), 1792, doi:10.1029/2002GL014819.

Roche, O., M. A. Gilbertson, J. C. Phillips, and R. S. J. Sparks (2004), Experimental study of gas-fluidized granular flows with implications for pyroclastic flow emplacement, *J. Geophys. Res.*, *109*, B10201, doi:10.1029/2003JB002916.

Scholten, F., et al. (2005), Mars express HRSC data processing, *Photogramm. Eng. Remote Sens.*, *71*(10), 1143–1152.

Sharp, R. P., and L. H. Nobles (1953), Mudflow of 1941 at Wrightwood, southern California, *GSA Bull.*, *64*(5), 547–560.

Shinbrot, T., N.-H. Duong, L. Kwan, and M. M. Alvarez (2004), Dry granular flows can generate surface features resembling those seen in Martian gullies, *Proc. Natl. Acad. Sci. U. S. A.*, *101*(23), 8542–8546.

Treiman, A. H. (2003), Geologic settings of Martian gullies: Implications for their origins, *J. Geophys. Res.*, *108*(E4), 8031, doi:10.1029/2002JE001900.

Védie, E., F. Costard, M. Font, and J. L. Lagarde (2008), Laboratory simulations of Martian gullies on sand dunes, *Geophys. Res. Lett.*, *35*, L21501, doi:10.1029/2008GL035638.

V. Ansan, N. Mangold, and V. Migeon, Laboratoire de Planétologie et Géodynamique de Nantes, Université de Nantes, CNRS, F-44322 Nantes, France. (nicolas.mangold@u-psud.fr)

D. Baratoux, Observatoire Midi-Pyrénées, Université Toulouse III, CNRS, F-31400 Toulouse, France.

F. Bouchut, École Normale Supériere, CNRS, F-75230 Paris, France.

A. Lucas and A. Mangeney, Institut de Physique du Globe de Paris, Université Paris Diderot 7, CNRS, F-75452 Paris, France.